Magneto-Mechanical Behavior Analysis using an Extended Jiles-Atherton Hysteresis Model for a Sheet Metal Blanking Application

Khaoula Hergli [1], Haykel Marouani [2], Mondher Zidi [1], and Yasser Fouad [2]

[1] Department of Mechanical Engineering
University of Monastir, LGM, Monastir, 5019, Tunisia
hergli.khaoula@gmail.com, mondher.zidi@enim.rnu.tn

[2] Department of Mechanical Engineering
King Saud University, P.O. Box 2454, Riyadh 11451, Saudi Arabia
hmarouani@ksu.edu.sa, yfouad@ksu.edu.sa

Abstract **—** Manufacturing processes affect the magnetic properties of the ferromagnetic components of electrical equipment. The optimization of the designed devices depends on two factors: the mechanical state of the material of a blanked part, especially near the cutting edge, and the magneto-mechanical behavior of the material used. In this paper we investigate the magnetic induction degradation of a blanked stator fabricated using fully processed, non-oriented Fe–(3 wt%)Si steel sheet. Owing to the geometric symmetry, we first simulated a half-stator teeth blanking using the Abaqus software. Subsequently, a magneto-mechanical extended Jiles–Atherton hysteresis model was used to determine the magnetic induction distribution on the blanked teeth stator. The numerical results show that the magnetic induction degradation can reach 25% upon applying moderate magnetic field, i.e., 1000 A/m, and 8% upon applying magnetic field close to the magnetic saturation, i.e., 3500 A/m. The depth of the affected region was approximately 1.25 mm before the material regained its initial magnetic state.

Index Terms **—** Blanking, finite element method, Jiles-Atherton hysteresis, magnetic properties, strain-magnetic coupling.

I. INTRODUCTION

Rotating electrical machines comprise ferromagnetic parts, which are manufactured using either conventional processes (blanking, drilling, shearing, etc.) or nonconventional ones (laser cutting or wire cutting). These processes, especially in ferromagnetic sheet metal forming, introduce local changes in the microstructure and generate internal stresses, thereby affecting the magnetic properties in the region of the cutting edge [1, 2] and increasing the magnetic losses near the cutting edge [3, 4]. Cao et al. [5] described the residual-stress distribution and magnetic domain structure on the cutting edge, demonstrating that the decrease in the width of the residual-stress-variation zone reduced the deterioration of magnetic properties. For punched ring structures, Lewis et al. [6] developed a simple model to represent the power loss as a function of the damaged-region width; The results showed that the power loss increased with decrease in the damaged width. Notably, elastic and plastic deformations significantly affect the magnetic properties of materials and alter the shape of the hysteresis curves. The elastic strain modifies the local internal nergy of the material, thereby affecting its magnetic behavior. However, compared with internal elastic stain, plastic deformations induce higher disorder in the magnetic behavior; therefore, the deterioration in magnetic properties is less noticeable over the elastic tensile stress range than that because of plastic deformation [7]. The adverse effects of plastic tension on magnetic properties are manifested in the range of the low plastic strain levels and in the low and medium magnetic field amplitudes [8–11]. The aforementioned phenomenon is more noticeable at high tensile stress, which results in increased losses [12]. Furthermore, the mechanical stresses affect magnetic anisotropy, decrease permeability, and increase power losses [10]. Blanking parameters (i.e., punch velocity and clearance) have also been investigated [13] to determine their contribution to the degradation of magnetic properties. Xiong et al. [14] demonstrated the mechanical-cutting-induced changes in the microstructure and texture of non-oriented Fe–Si, deterioration in its magnetic properties, and a significant change in the resulted hysteresis loop. They also reported that these variations were more apparent upon increasing the cutting length per mass. Wang et al. [15] and Kuo et al. [16] revealed the importance of punching clearance, which deteriorates the magnetic performance. In addition, Weiss et al. [17] demonstrated that smaller cutting clearances could result in higher residual stresses near the cutting surface. They further showed that both

Submitted On: February 3, 2020
Accepted On: April 19, 2020

1054-4887 © ACES

important cutting speed and wear of the tool increased the losses and deteriorated magnetization. Furthermore, material characteristics of electrical steels, such as thickness, grain size, and crystallographic texture strongly affect the magnetic properties of non-oriented electrical steel sheets [18]. Kuo et al. [16] indicated that a material with small grain size had low deformation during the punching process. Omura et al. [19] and Toda et al. [20] studied the effect of the hardness and thickness of non-oriented electrical steels on iron-loss deterioration by blanking process and, consequently, observed that material iron loss was low in thin or hard specimens.

Establishing a description for multiple physical coupling processes is essential. Several models have been developed and implemented into a numerical model to define the magneto-mechanical behavior of ferromagnetic materials in electrical devices. Coupling was employed to study the effect of blanking on the magnetic response [10] and the contribution of multiaxial stress on magnetization [10,11,13,21]. A certain amount of coupling was proposed as an extension of existing classical magnetic hysteresis models [13,22–24]. The numerical modeling of such problems requires sufficient computer capacity, powerful software for the simulations, and a well-defined and efficient approach. However, all of the cited studies have limitations. The coupled model of Ossart et al. [10] is based on the conversion of the local microhardness into an equivalent plastic strain, which cannot describe the complex state induced by blanking. Bernard and Daniel [13] extended the Jiles–Atherton (J–A) hysteresis model by introducing mechanical stress via anhysteretic magnetization and by modifying the pinning factor. This model was then implemented into a time-stepping finite element method. However, this approach suffers from critical convergence difficulties. The multiscale approach used by Aydin et al. [21] and based on the free energy in the domain scale is also insufficient, as it relies on only a few material parameters and provides a description of the coupled magneto-mechanical anhysteretic behavior only.

In this work, we present a coupled experimental and numerical analysis of magnetic behavior degradation for stator teeth blanking. Magnetic experiments on ferromagnetic sheet steel were carried out at different levels of plastic strain to develop an extended J–A hysteresis model considering the strain-magnetic field coupling. A sheet metal blanking model of a half-teeth stator was developed and validated using the Abaqus software. Then, a coupling analysis using Python and Abaqus was performed. The Python code obtained the plastic strain map from the finite element simulation and calculated the corresponding magnetic induction for a given magnetic field. These values were inserted in the teeth stator part to visualize the magnetic induction and distribution of degradation. An analysis performed close to the cutting edge revealed the "magnetic dead zone" depth.

II. THE JILES-ATHERTON HYSTERESIS MODEL

Jiles and Atherton [25] defined the total magnetization M as the sum of two components:

$$M = M_{rev} + M_{irr}, \tag{1}$$

where M_{rev} is the reversible component resulting from the deformation of the walls on the coupling sites under the action of an external field and M_{irr} represents the irreversible magnetization. They can be analyzed by the set of differential equations:

$$\begin{cases} \dfrac{dM_{rev}}{dH} = c\left(\dfrac{dM_{an}}{dH} - \dfrac{dM_{irr}}{dH}\right) \\ \dfrac{dM_{irr}}{dH} = \dfrac{M_{an} - M_{irr}}{\delta\, k - \alpha(M_{an} - M_{irr})} \end{cases}, \tag{2}$$

where c is the coefficient of reversibility in the range of 0–1, H is the applied magnetic field, δ is the directional parameter, taking the value of +1 or −1, α is the domain coupling parameter, and k is the pinning factor. The anhysteretic magnetization is denoted by M_{an} and it can be expressed by the modified Langevin function:

$$M_{an} = M_s\left(\coth\left(\frac{H_e}{a}\right) - \frac{a}{H_e}\right), \tag{3}$$

where a represents the domain density, M_s is the saturation magnetization and H_e is the Weiss effective field given by:

$$H_e = H + \alpha M. \tag{4}$$

Considering all these expressions, the J–A hysteresis model can be expressed by the differential equation:

$$\frac{dM}{dH} = (1-c)\frac{M_{an} - M_{irr}}{\delta k - \alpha\left(M_{an} - M_{irr}\right)} + c\frac{dM_{an}}{dH}, \tag{5}$$

which is a function of five parameters $\{M_s, a, \alpha, c, k\}$.

III. EXPERIMENTAL ASPECTS OF MAGNETO-MECHANICAL COUPLING

In this section, we present the experimental arrangement for the magnetic measurements, the obtained magnetic hysteresis at different levels of plastic strain, and the developed theoretical model based on the J–A hysteresis model, which considers the magneto-mechanical behavior coupling. It should be noted that a more detailed description of the magnetic measurement test apparatus is available in Refs. [22,26].

A. Arrangement for magnetic measurements

The samples were obtained from a fully processed, non-oriented Fe–(3 wt%)Si steel sheet with a thickness of 0.35 mm. The magnetic measurements were carried out in the "initial state" (i.e., without residual stress) and in the "loaded state" (i.e., different ranges of plastic strain applied up to 10% using a universal testing machine). The applied stress and the magnetic field were

both in the rolling direction.

Figure 1 shows the obtained experimental hysteresis loop at different loaded states. The total strain is assumed to be plastic strain under a static regime (frequency of 1 Hz). As can be seen in Fig. 1, the magnetic properties are affected even at a low range of deformation. For example, it is noticeable that the magnetization at saturation and the remanence decrease with the increase in the deformation. Saturation is the state reached when an increase in the applied external magnetic field cannot increase the magnetization of the material and remanence is the magnetic flux density remaining in a material following the removal of the magnetizing field. However, the coercive field and hysteresis losses increase with the increase in the deformation. Magnetic coercivity is a measure of the ability of a ferromagnetic material to withstand an external magnetic field without becoming demagnetized and the hysteresis loss is proportional to the area of the hysteresis loop.

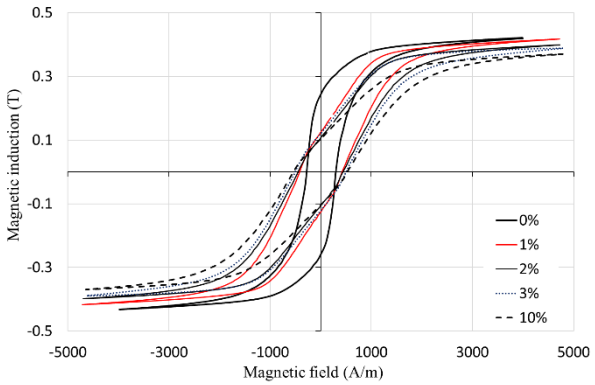

Fig. 1. Experimental hysteresis loops as functions of the applied elastoplastic deformation [23].

B. Hysteresis simulation

Several efforts have been made to develop hysteresis models suitable for different materials and frequencies. In our study, we employed the J–A model [22,25]. The implementation of such a model requires the identification of five parameters: the saturation magnetization, the domain-coupling parameter, the pinning factor, the coefficient of reversibility, and the domain density. The J–A parameters were successfully identified using a genetic algorithm procedure for each plastic strain range [22]. A parameter sensitivity investigation allowed us to assume that parameter a had the greatest effect on the shape of the hysteresis curve. The study of the evolution of the J–A model parameters for different elastoplatic deformations reveals that only the domain density a depends on the deformation. The results of the hysteresis curve simulation for non-deformation, low deformation, and even at high deformation, with α, c, and k constants, are in agreement with the measurements. Accordingly, we assume that they are independent of the elastoplastic deformation. Then, only parameter a is expected to be a function of εp and follows the law:

$$a = \frac{119 + 650.\varepsilon_p}{1 + \varepsilon_p}. \tag{6}$$

For the three other J–A parameters, we averaged the centered values of ten genetic algorithm simulations: $\alpha = 150 \times 10^{-6}$, $c = 31 \times 10^{-3}$, and k = 498 A/m. Figure 2 shows the experimental and simulated hysteresis for the initial state and 10% of mechanical deformation. Compared with the experimental results, all simulation results show a mean square error of less than 5%.

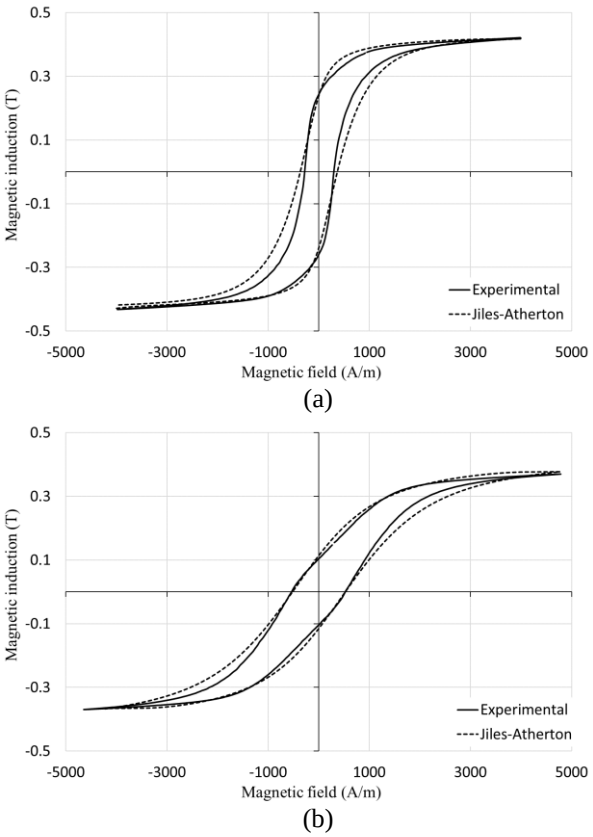

Fig. 2. Measured and simulated hysteresis loops for Fe–(3wt%)Si at different elastoplastic deformations (a) 0% and (b) = 10%) [22].

IV. NUMERICAL ASPECTS OF STATOR TEETH BLANKING

In this section, we present the finite element analysis of a half-teeth stator blanking by using the Abaqus software.

A. Finite element model

Figure 3 depicts the different tools employed for the simulation of the stator teeth blanking, where, owing to its geometric symmetry, only a half part is included. The

half blank, which was rectangular, with dimensions 115 mm × 45 mm × 0.8 mm, was positioned between a die and blank holder. All the process tools had a fitting radius of 0.2 mm. The radial clearance between the punch and die, relative to the sheet thickness, was 10% (sheet thickness equal to 1.2 mm). The model of the tools was based on the application of rigid bodies. The die and blank holder were fixed, and the punch moved at 100 mm/s. The contact was described using a Coulomb friction model with a friction coefficient, μ, of 0.18.

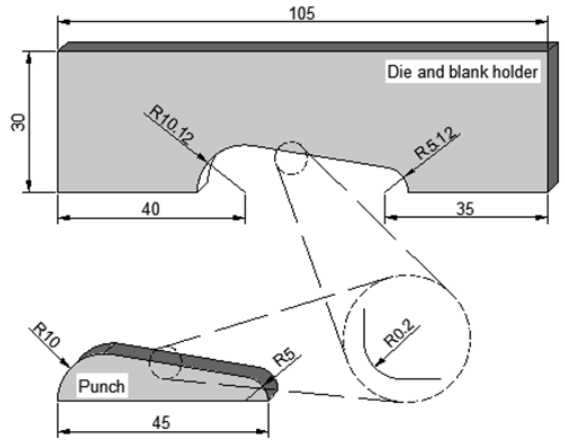

Fig. 3 Geometric description of the blanking tools.

The material investigated was a 1.2-mm-thick sheet of isotropic non-oriented full-process Fe–(3 wt%)Si steel. Various tensile tests were performed at the strain rate of 10^{-5} s^{-1}. This value of strain rate is, generally, used to describe the "quasi-static" behavior of the material. The material work hardening can be described using a conventional Ludwik's law. The quasi-static yield stress is given as follows:

$$\bar{\sigma}_0(\bar{\varepsilon}_p) = 770(\bar{\varepsilon}_p)^{0.26} . \quad (7)$$

While assuming the quasi-static material behavior, we do not consider the high magnitude of the punch velocity. Therefore, it is better to improve the material-behavior description using a strain-rate-behavior law. In such a model, the rate of the effective plastic strain is related to the difference between the current stress and yielding stress, as proposed by Peirce et al. [27]. For one-dimensional rate-dependent plasticity and isotropic work hardening, the effective plastic strain rate is given as:

$$\dot{\bar{\varepsilon}}^p = \dot{\bar{\varepsilon}}_0^p \left(\frac{|\sigma|}{\bar{\sigma}(\bar{\varepsilon}^p)} \right)^m , \quad (8)$$

where $\bar{\varepsilon}^p$ is the equivalent plastic strain, $\dot{\bar{\varepsilon}}^p$ is the equivalent plastic strain rate, which is the reference strain rate used to measure the quasi-static yield stress, and m is the rate sensitivity parameter (m > 0).

As the blanking process is not time-dependent, the dependence on the strain rate is considered using the rate-dependent yield. When the dependences on the strain and strain rate are assumed to be separable and isotropic work hardening is considered, the strain rate dependent yield-stress $\bar{\sigma}$ is defined by:

$$\bar{\sigma}(\bar{\varepsilon}^p, \dot{\bar{\varepsilon}}^p) = \bar{\sigma}_0(\bar{\varepsilon}^p) \left(\frac{\dot{\bar{\varepsilon}}^p}{\dot{\bar{\varepsilon}}_0^p} \right)^m , \quad (9)$$

where $\bar{\sigma}_0(\bar{\varepsilon}^p)$ is the quasi-static yield stress at the quasi-static strain rate $\dot{\bar{\varepsilon}}_0^p$.

To study the strain rate sensitivity, the true stress–strain curves were measured using an Instron test machine equipped with a charge-coupled device (CCD) camera and a data acquisition system controlling the prescribed displacement to maintain a constant strain rate in the center of the specimen. The technique used for these video controlled tests is based on the procedure developed by G'sell and Jonas [28]. The experimental arrangement was used to perform tensile tests at different strain rates ranging from 10^{-5} to 5 $\times 10^{-3}$ s^{-1}, with a reference strain rate set as 10^{-5} s^{-1}. The result obtained for the investigated material shows a significant strain rate sensitivity value (m = 0.0085).

The numerical simulation of the sheet metal blanking process has been reported by several studies [2,29,30] Different approaches have been proposed to simulate the shearing process and to treat ductile fracture. In this work, we use the non-iterative explicit approach to model the high nonlinearity associated with the blanking process. An arbitrary Euler–Lagrange formulation was employed to treat the large mesh distortion occurring during the calculation and leading to strain localization and mesh degradation, resulting in significant errors. The blank is meshed using 22 610 hexahedral elements with reduced integration (type C3D8R), as shown in Fig. 4.

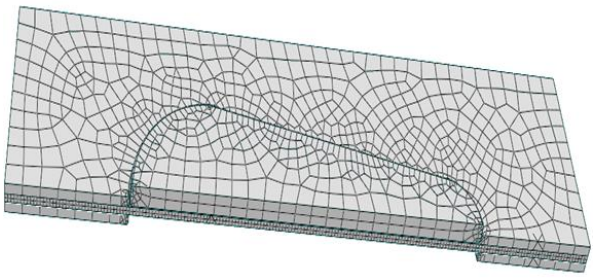

Fig. 4. Finite element model for the blanking test simulation.

Among the several existing sheet metal-forming processes, the blanking process is special in the respect that plastic straining is followed by ductile fracture and material separation. We used the well-known

Gurson–Tvergaard–Needleman model [31,32] to treat ductile fracture. The nine Gurson–Tvergaard–Needleman parameters are summarized in Table 1 [2,29], where term f_0 is the initial void fraction, $\{q_1, q_2, q_3\}$ are adjustable material parameters, f_N is the volume fraction of the nucleating void, ε_N is the mean strain for void nucleation, S is the standard deviation, f_c is the critical void volume fraction, and f_F is the void volume fraction at failure.

Table 1: Gurson–Tvergaard–Needleman parameters

f_0	q_1	q_2	q_3	ε_N	f_N	S	f_c	f_F
0.01	1.5	1	2.25	0.3	0.04	0.1	0.11	0.12

B. Finite element results

Because of the lack of experimental tests on stator teeth blanking, the validation of our numerical approach is based only on the numerical punch displacement as a function of the punch load. According to the literature, the maximum blanking load, F_{max}, is expressed by [33]:

$$F_{max} = k.P.e.\sigma_{max}, \quad (10)$$

where k is a calibration factor ($0.8 < k < 0.95$), P is the perimeter of the punch, e is the thickness of the blank, and σ_{max} is the maximum tensile stress of the material.

According to equation (10), the maximum load needs to be in the range of 13.0–15.5 kN. In addition, for steel case blanking, fracture typically occurs between 85 and 95% of the thickness of the sheet [29]. These findings are confirmed by the curve of the simulated penetration as a function of load (Fig. 5). A reference point was assigned to the punch (rigid body) which enabled the acquisition of the tool displacement and total punch force required to penetrate the blank. The relative punch displacement is defined as the ratio of punch displacement and the blank thickness.

Figure 6 shows the von Mises stress distribution and the "equivalent plastic strain" (PEEQ) distribution.

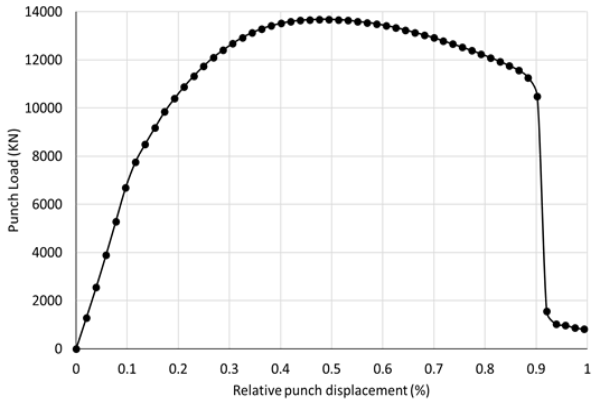

Fig. 5. Teeth stator load as a function of displacement (maximum load = 13 685 N; relative displacement at fracture = 0.88).

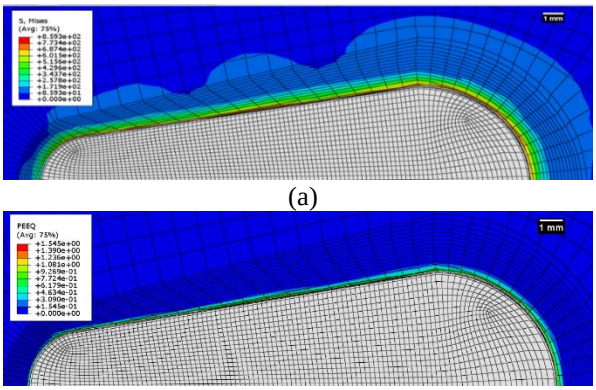

Fig. 6. (a) von Mises stress distribution, and (b) PEEQ distribution.

V. APPLICATION OF THE MAGNETO-MECHANICAL COUPLING

The magneto-mechanical coupling is realized following different steps and using the Abaqus software and a model in Python language. Figure 7 shows the applied numerical procedure. First, a blanking finite element simulation of the half-teeth stator is performed as described in the previous section. Then, the value of the equivalent plastic strain for each element of the specimen mesh is obtained. For a given value of magnetic field, H, we calculate the corresponding value of the magnetic induction using the extended J–A formulation (see section "Materials and Methods"). Two new variables are created and saved in the odb file used by Abaqus. The first variable is denoted as "magnetic induction," describing the magnetic distribution through the blanked part [Fig. 8 (a) and 9 (a)]. The second variable is denoted as "degradation," representing the relative degradation of the magnetic induction, and it corresponds to the percentage rate of corresponding magnetic induction and maximum magnetic induction [Fig. 8 (b) and Fig. 9 (b)].

Figure 8 and Fig. 9 show that far from the cutting edge, the material regains its original magnetic properties. For the better analysis of the magnetic efficiency and to provide guidance for electrical parts designers, it is important to characterize the magnetic properties near the cutting edge and to determine the width of the affected area. For this purpose, we defined two "paths," shown in Fig. 10, to analyze the evolution of the magnetic properties near the cutting edge. The results summarized in Fig. 11 show that the magnetic degradation is more substantial for the low and medium range magnetic fields: the magnetic induction degradation reached 23.8% for an applied magnetic field of 1000 A/m. Close to the magnetic saturation (H_s = 4500 A/m), the degradation is less severe: the magnetic induction degradation reached 7.4% for an applied magnetic field

of 3500 A/m. The affected area is approximately 1.25 mm for all cases.

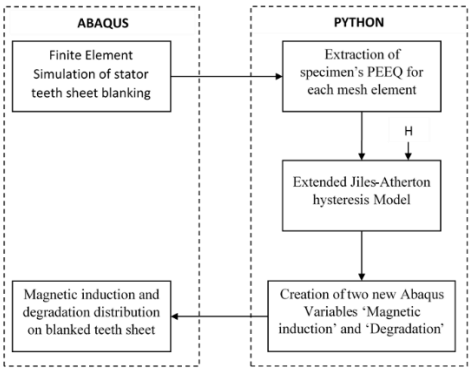

Fig. 7. Flowchart of the magneto-mechanical coupling process.

Figure 8 and Fig. 9 represent the magnetic flux distribution and the corresponding degradation for two magnetic field values, H = 1000 A/m and H = 3500 A/m, respectively.

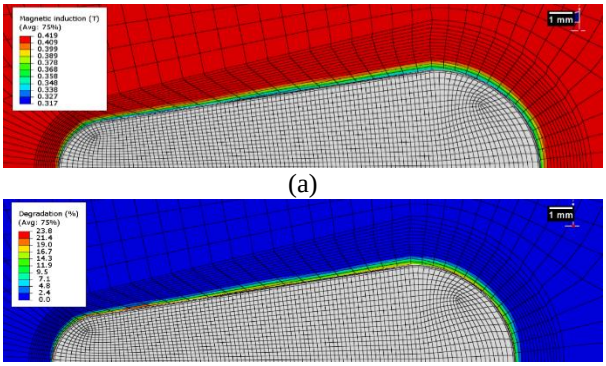

(a)

(b)

Fig. 8. Simulation at magnetic field of H = 1000 A/m: (a) Magnetic induction distribution and (b) degradation.

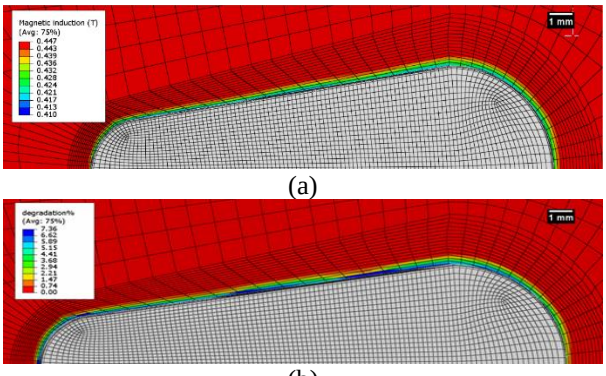

(a)

(b)

Fig. 9. Simulation at magnetic field of H = 3500 A/m: (a) Magnetic induction distribution and (b) degradation.

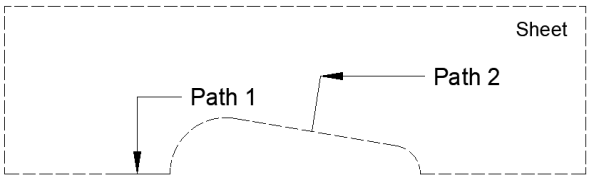

Fig. 10. Paths for monitoring the magnetic induction evolution.

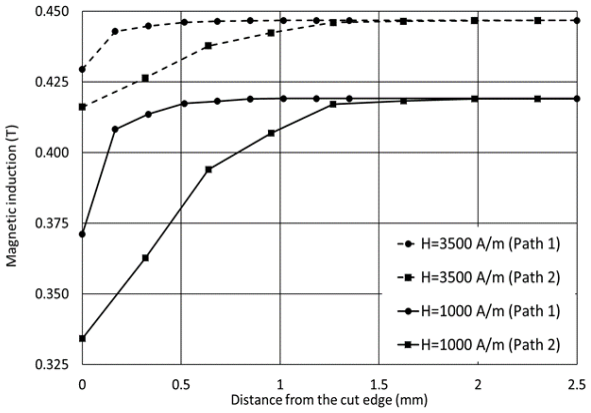

Fig. 11. Magnetic induction evolution along different paths.

VI. CONCLUSION

We performed both experimental and numerical studies on the magneto-mechanical coupling and applied them to stator blanking. The finite-element simulation of a teeth stator using the Gurson–Tvergaard–Needleman constitutive model and an arbitrary Euler–Lagrange mesh description were performed to obtain the accurate plastic strain distribution on the blanked part. A static model of a fully processed, non-oriented Fe–(3 wt%)Si steel sheet under plastic strain was developed on the basis of the classical J-A hysteresis model. In addition, genetic algorithms were used to identify the hysteresis model parameters and formulate an extended description of the J–A model. Using Python language, a simulation procedure was developed. First, the plastic strain state was obtained using the Abaqus process. Subsequently, we analyzed the magnetic induction corresponding to a given value of magnetic field. Finally, both the magnetic induction and magnetic degradation were described using the Abaqus software. From the results, it was evident that the magnetic degradation could reach 25% for a moderate value of the applied magnetic field, and that the width of the "magnetic dead zone" approached 1.25 mm near the cutting edge before the material regained its initial magnetic state. The developed procedure is a helpful tool for engineers and electrical equipment designers to optimize the performance of their electrical designs.

ACKNOWLEDGMENT

The authors would like to extend their sincere appreciation to the Deanship of Scientific Research at the King Saud University for its funding of this research through the Research Group [No. RG-1439/007].

REFERENCES

[1] H. M. S. Harstick, M. Ritter, and W. Riehemann, "Influence of punching and tool wear on the magnetic properties of monoriented electrical steel," *IEEE Transactions on Magnetics*, vol. 50, no. 4, 2014.

[2] H. Marouani, A. Ben Ismail, E. Hug, and M. Rachik, "Rate-dependent constitutive model for sheet metal blanking investigation," *Materials Science and Engineering A*, vol. 487, no. 1-2, pp. 162-170, 2008.

[3] H. Naumoski, B. Riedmüller, A. Minkow, and U. Herr, "Investigation of the influence of different cutting procedures on the global and local magnetic properties of non-oriented electrical Steel," *Journal of Magnetism and Magnetic Materials*, vol. 392, pp. 126-133, 2015.

[4] H. Naumoski, A. Maucher, L. Vandenbossche, et al., "Magneto-optical and field-metric evaluation of the punching effect on magnetic properties of electrical steels with varying alloying content and grain size," *in 2014 4th International Electric Drives Production Conference (EDPC)*, Nuremberg, pp. 1-9. 2014.

[5] H. Cao, L. Hao, J. Yi, et al., "The influence of punching process on residual stress and magnetic domain structure of non-oriented silicon steel," *Journal of Magnetism and Magnetic Materials*, vol. 406, pp. 42-47, 2016.

[6] N. Lewis, P. Anderson, J. Hall, and Y. Gao, "Power loss models in punched non-oriented electrical steel rings," *IEEE Transactions on Magnetics*, vol. 52, no 5, pp. 1-4, 2016.

[7] N. Leuning, S. Steentjes, M. Schulte, W. Bleck, and K. Hameyer, "Effect of elastic and plastic tensile mechanical loading on the magnetic properties of NGO electrical steel," *Journal of Magnetism and Magnetic Materials*, vol. 417 pp. 42-48, 2016.

[8] V. E. Iordache and E. Hug, "Effect of mechanical strains on the magnetic properties of electrical steels," *Journal of Optoelectronics and Advanced Materials*, vol. 6, no. 4, pp. 1297-1303, 2004.

[9] V. E. Iordache, F. Ossart, and Eric Hug, "Magnetic characterisation of elastically and plastically tensile strained non-oriented Fe-3.2%Si steel," in *Journal of Magnetism and Magnetic Materials*, vol. 254-255, pp. 57-59, 2003.

[10] F. Ossart, E. Hug, O. Hubert, C. Buvat, and R. Billardon, "Effect of punching on electrical steels: Experimental and numerical coupled analysis," in *IEEE Transactions on Magnetics*, vol. 36, no. 5, pp. 31370-3140, 2000.

[11] M. Rekik, O. Hubert, and L. Daniel, "Influence of a multiaxial stress on the reversible and irreversible magnetic behaviour of a 3%Si-Fe alloy," in *International Journal of Applied Electromagnetics and Mechanics*, vol. 44, no. 3-4, pp. 301-315, 2014.

[12] H. Naumoski, A. Maucher, and U. Herr, "Investigation of the influence of global stresses and strains on the magnetic properties of electrical steels with varying alloying content and grain size," *2015 5th International Conference on Electric Drives Production, EDPC 2015 – Proceedings*, pp. 1-8, 2015.

[13] L. Bernard and Laurent Daniel, "Effect of stress on magnetic hysteresis losses in a switched reluctance motor: Application to stator and rotor shrink fitting," *IEEE Transactions on Magnetics*, vol. 51, no. 9, pp. 1-13, 2015.

[14] X. Xiong, S. Hu, K. Hu, and S. Zeng, "Texture and magnetic property evolution of non-oriented Fe-Si steel due to mechanical cutting," *Journal of Magnetism and Magnetic Materials*, vol. 401, pp. 982-990, 2016.

[15] Z. Wang, S. Li, R. Cui, X. Wang, and B. Wang, "Influence of grain size and blanking clearance on magnetic properties deterioration of non-oriented electrical steel," *IEEE Transactions on Magnetics*, vol. 54, no. 5, pp. 1-7, 2018.

[16] S. Kuo, W. Lee, S. Lin, and C. Lu, "The influence of cutting edge deformations on magnetic performance degradation of electrical steel," *IEEE Transactions on Industry Applications*, vol. 51, no 6, pp. 4357-4363, 2015.

[17] H. A. Weiss, N. Leuning, S. Steentjes, et al., "Influence of shear cutting parameters on the electromagnetic properties of non-oriented electrical steel sheets," *Journal of Magnetism and Magnetic Materials*, vol. 421, pp. 250-259, 2017.

[18] Y. Zaizen, T. Omura, M. Fukumura, K. Senda, and H. Toda, "Evaluation of stress distribution due to shearing in non-oriented electrical steel by using synchrotron radiation," *AIP Advances*, vol. 6, no. 5, 055926, 2016.

[19] T. Omura, Y. Zaizen, M. Fukumura, K. Senda, and H. Toda, "Effect of hardness and thickness of nonoriented electrical steel sheets on iron loss deterioration by shearing process," *IEEE Transactions on Magnetics*, vol. 51, no. 11, pp. 1-4, 2015.

[20] H. Toda, "Iron loss deterioration by shearing process in non-oriented electrical steel with different thicknesses and its influence on estimation of motor iron loss," *IEEJ Journal of Industry Applications*, vol. 3, no. 1, pp. 55-61, 2013.

[21] U. Aydin, P. Rasilo, F. Martin, et al., "Magneto-mechanical modeling of electrical steel sheets," *Journal of Magnetism and Magnetic Materials*, vol. 439, pp. 82-90, 2017.
[22] K. Hergli, H. Marouani, and M. Zidi, "Numerical determination of Jiles–Atherton hysteresis parameters: Magnetic behavior under mechanical deformation," *Physica B: Condensed Matter*, vol. 549, pp. 74-81, 2018.
[23] F. Sixdenier, O. Messal, A. Hilal, et al., "Temperature-dependent extension of a static hysteresis model," in *IEEE Transactions on Magnetics*, vol. 52, no. 3, pp. 1-4, 2016.
[24] R. Szewczyk and P. Frydrych, "Extension of the Jiles-Atherton model for modelling the frequency dependence of magnetic characteristics of amorphous alloy cores for inductive components of electronic devices," in *Acta Physica Polonica A*, vol. 118, no. 5, pp. 782–784, 2010.
[25] D. C. Jiles and D. L. Atherton, "Theory of ferromagnetic hysteresis," *Journal of Magnetism and Magnetic Materials*, vol. 61, no. 1-2, pp. 48-60, 1986.
[26] K. Hergli, H. Marouani, M. Zidi, Y. Fouad, and M. Elshazly, "Identification of Preisach hysteresis model parameters using genetic algorithms," *Journal of King Saud University - Science*, 2018.
[27] D. Peirce, C. F. Shih, and A. Needleman, "A tangent modulus method for rate dependent solids," *Computers and Structures*, vol. 18, no 5, pp. 875-887, 1984.
[28] C. G'sell and J. J. Jonas, "Determination of the plastic behaviour of solid polymers at constant true strain rate," *Journal of Materials Science*, vol. 14, no. 3, pp. 583-591, 1979.
[29] H. Marouani, A. Ben Ismail, E. Hug, and M. Rachik, "Numerical investigations on sheet metal blanking with high speed deformation," *Materials and Design*, vol. 30, no. 9, pp. 3566-3571, 2009.
[30] H. Marouani, M. Rachik, and E. Hug, "Experimental investigations and FEM simulations of parameters influencing the Fe-(Wt.3%)Si shearing process," *Mechanics & Industry*, vol. 13, no. 4, pp. 271-278, 2012.
[31] A. L. Gurson, "Continuum theory of ductile rupture by void nucleation and growth: Part I—Yield criteria and flow rules for porous ductile media," *Journal of Engineering Materials and Technology*, vol. 99, no. 1, pp. 2-15 1977.
[32] V. Tvergaard, "Influence of voids on shear band instabilities under plane strain conditions," *International Journal of Fracture*, vol. 17, no. 4, pp. 389-407, 1981.
[33] H. Derterme and A. Maillard, *Données Métier En Découpage: Quantification de l'influence de La Vitesse de Découpage*. edited by R. D'étude, CETIM, 1997.

Khaoula Hergli was born in Tunisia on November 15, 1986. She received the engineering degree and the master diploma in Mechanical Engineering from the National college of Engineers of Monastir in Tunisia, in 2011 and 2013, respectively.

She is currently a Ph.D. student in the Laboratory of Mechanical Engineering at the National college of Engineers of Monastir since December 2015. She has focused her researches on magnetic hysteresis modeling of soft magnetic materials, sheet metal-forming processes and multiphysics coupling.

Haykel Marouani was born in Tunis, Tunisia, in 1978. He received the B.E. degree in Mechanical Engineering from the National Engineering College of Monastir (Tunisia) in 2001. He received the M.E. and Ph.D. degree from the University of Technology of Compiegne in 2002 and 2006, respectively. He has been the Head of the Mechanical Department of the National Enginering College of Monastir from 2011 to 2014. He is currently working at King Saud University (Saudi Arabia). His main research areas of interest are ferromagnetic sheet metal forming, especially by punching, piercing, and shearing.